Coding and Decoding Stray Magnetic Fields for Multiplexing Kinetic Bioassay Platform

Yuan Liu[1,2†], Gungun Lin[1,2†], Yinghui Chen[1,2], Ingolf Mönch[3], Denys Makarov[3], Bradley J. Walsh[2,4], Dayong Jin[1,2,5]

1. Institute for Biomedical Materials and Devices, Faculty of Science, The University of Technology Sydney, Ultimo, New South Wales 2007, Australia
2. ARC Research Hub for Integrated Device for End-User Analysis at Low Levels, Faculty of Science, University of Technology Sydney, Sydney, NSW 2007, Australia
3. Helmholtz-Zentrum Dresden-Rossendorf e.V., Institute of Ion Beam Physics and Materials Research, Bautzner Landstrasse 400, 01328, Dresden, Germany
4. Minomic International Ltd, Macquarie Park, NSW 2113, Australia
5. UTS-SUStech Joint Research Centre for Biomedical Materials & Devices, Department of Biomedical Engineering, Southern University of Science and Technology, Shenzhen, China

†: these authors contributed equally to this work
Correspondence addressed to: gungun.lin@uts.edu.au &dayong.jin@uts.edu.au

This supplementary file includes the following:

Supplementary Section 1: Magnetostatic simulation of stray field patterns

Figure S1 | Computational simulation of the stray magnetic field of magnetically permeable structures

Supplementary Section 2: Stability test of polymeric composites

Table S1 | Stability test of pure alginate polymeric structures in various biochemical buffers

Figure S2 | Chemical buffer stability optimization of polymer composition for the fabrication of bio-interfacing microparticle composite

Supplementary Section 3: Purpose-built micro-electromagnetoelectrical decoding systems

Figure S3 | Schematic of the electrical measurement setup

Figure S4 | Fabrication of a magnetofluidic decoder

Supplementary Section 4: DNA sequences for viruses used for biochemical assays

Table S2 DNA sequences for viruses used for biochemical assay

Supplementary Section 5: Chracterization of magnetic material

Supplementary Section 1: Magnetostatic simulation of stray field patterns
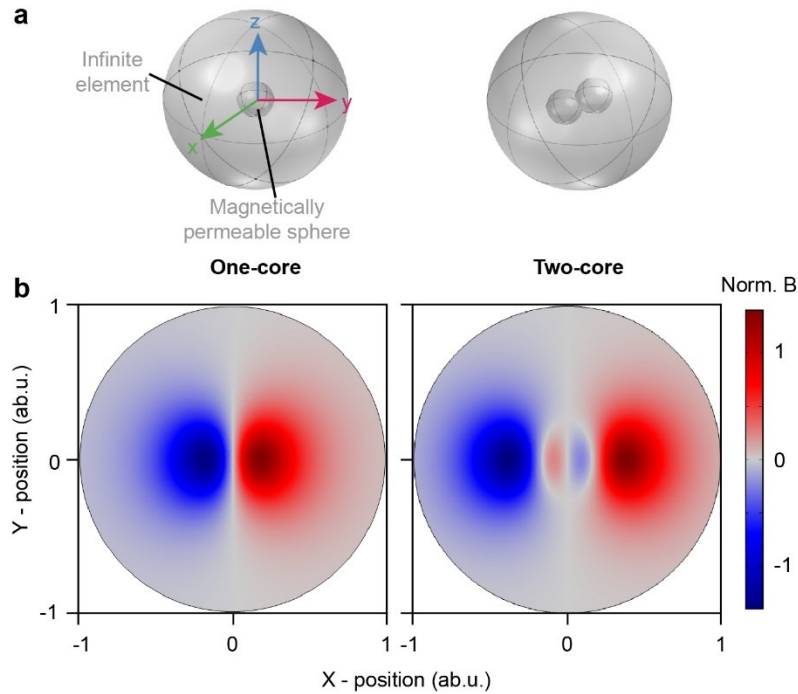

Figure S1 | Computational simulation of the stray magnetic field of magnetically permeable structures. (a) One-core and dual-core magnetic structures are simulated as one-core and dual-core magnetically permeable spheres using the software COMSOL Multiphysics. The sphere is exposed to a spatially uniform static background magnetic field of strength of 1 mT, applied along the z axis. The computational model consists of three concentric spheres. We define the innermost as the magnetically permeable sphere, the surrounding spherical shell as free space, and the outside shell as a region extending to infinity which was modelled with an *Infinite Element Domain*. We used the scalar potential formulation in the *Magnetic Fields, No Currents* interface, to solve the magnetic flux conservation equation: $\nabla \cdot \mathbf{B} = 0$. A partial differential equation for the magnetic scalar potential field, $\mathbf{V}_m$ can be expressed as: $\nabla \cdot \mu_r \mu_0 (-\nabla \mathbf{V}_m + \mathbf{H}_b) = 0$, where the background field is described by the $\mathbf{H}$-field, $\mathbf{H}_b$. The $\mathbf{B}$-field was then computed from the H-field: $\mathbf{B} = \mu_r \mu_0 \mathbf{H}$. The H-magnetic field was in turn computed from the gradient of the magnetic scalar potential, $\mathbf{V}_m$. (b) Simulated stray magnetic field distribution projected on the x-y plane for the two types of microstructures.

Supplementary Section 2: Stability test of polymeric composites

Table S1 – Stability test of pure alginate polymers in various biochemical buffers*

PBS	Tris	Tris (with 20mM CaCl$_2$)	Tris (with 100mM CaCl$_2$)	MES	MES (with 20mM CaCl$_2$)	MES (with 100mM CaCl$_2$)	HEPES	HEPES (with 20mM CaCl$_2$)	HEPES (with 100mM CaCl$_2$)
150mM NaCl$_2$ PH 7.5	150mM NaCl$_2$, PH>7			PH<6				PH 7.1	
Degradation	Stable	Stable	Swelling	Stable	Stable	Swelling	Stable	Stable	Stable

*The stability of pure alginate particles in various biochemical buffers are tested. Different buffers for bio-conjugation and assays may involve Na$^+$ ions that can replace Ca^{2+} ions in the alginate, which causes the degradation of the polymer.[1] We show that adding Ca^{2+} in different buffers can effectively stabilize the polymers for the long-term storage and application of alginate-incorporated composite polymer microstructures.
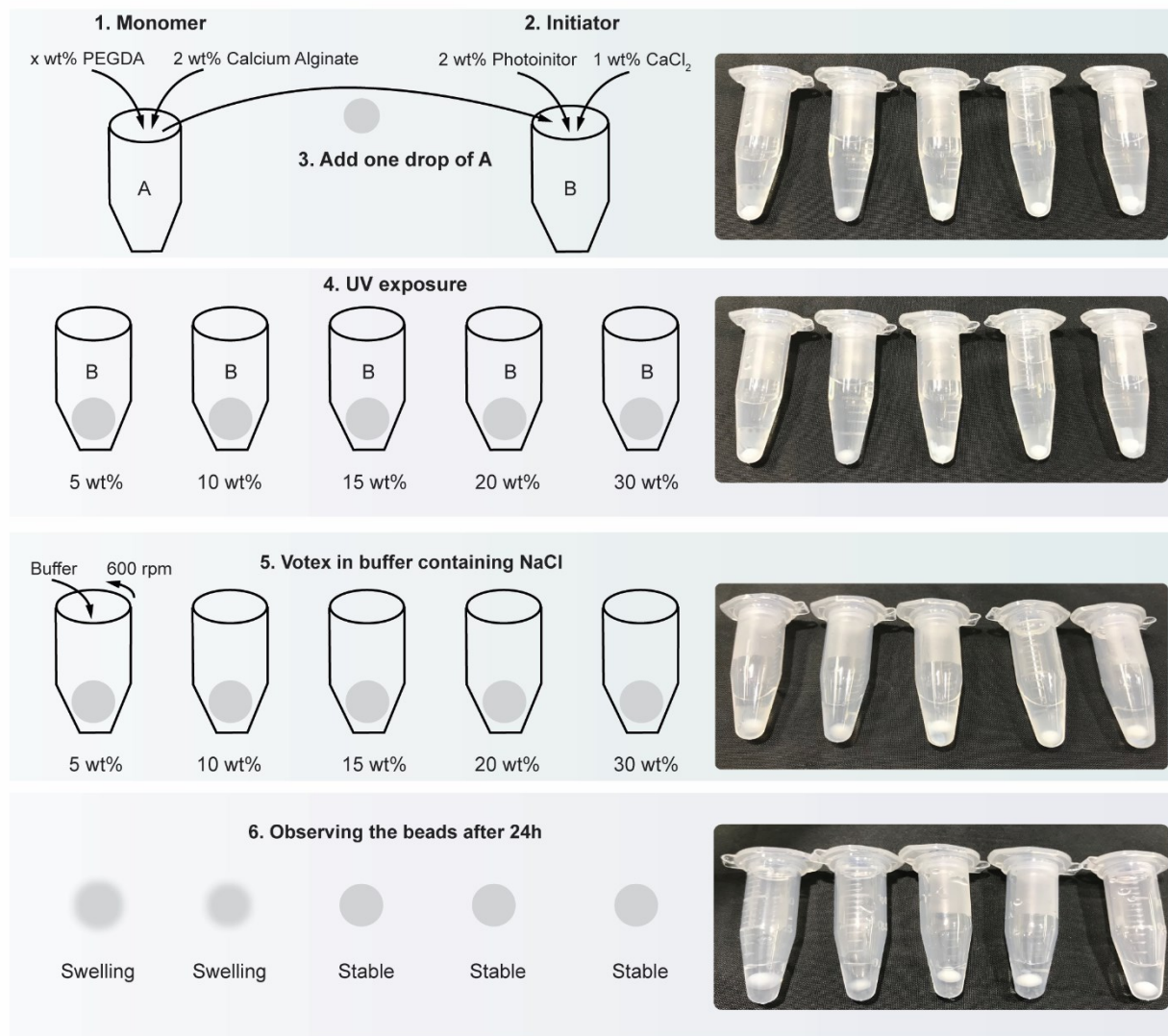
Figure S2 | Chemical buffer stability testing of polymer composition for the fabrication of microparticle composite. a. Experimental process for the testing the stability of polymer compositions using different wt% of PEGDA and 2wt% alginate. A drop of the polymer composite is added in a solution containing 2wt% photo initiator and 1% $CaCl_2$, followed by UV illumination. The resultant polymeric composites are added in a buffer containing 150mM $NaCl_2$. After 24h vortex in the buffer, the stability of the composites is compared. It is shown that up to 15 wt% of PEGDA is needed to prevent the composites from swelling.

Supplementary Section 3: Purpose-built micro-electromagnetoelectrical decoding systems
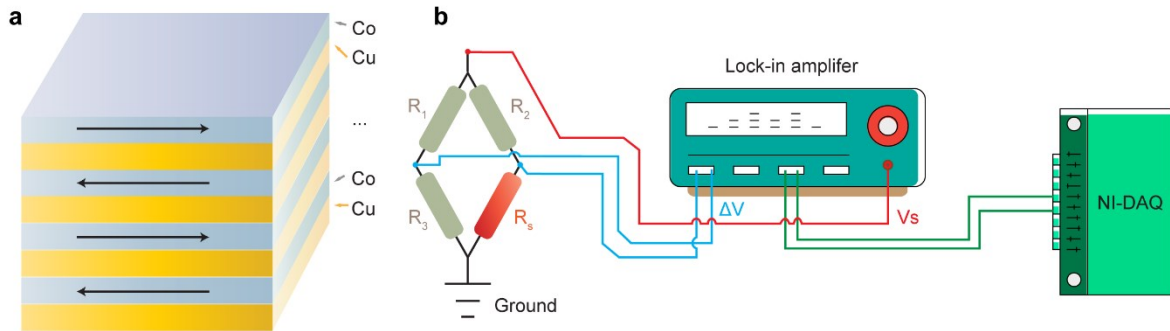

Figure S3 | Schematic of the electrical measurement setup. (a) Schematic illustration of GMR multilayer stack consisting of Co (1 nm)/ [Co (1 nm)/Cu (1 nm)]$_{50}$/Ta (5 nm) were deposited on the glass substrate by magnetron sputtering using Ar as a sputter gas (pressure of Ar = 9×10^{-4} mbar. Base pressure: 9×10^{-8} mbar). Electrical contacts of Au (75 nm)/Cr (5 nm) were deposited using electron beam evaporation at room temperature (base pressure 10^{-7}mbar). (b) Electrical measurement circuit. The GMR sensor (R_s) was included in a Wheatstone bridge circuit with other trimmers (R_1, R_2 and R_3). This bridge was powered directly by the AC voltage source (maximum: 5V) of a lock-in. The voltage was adjusted so that 1mA current was flowing through the sensor. The trimmers were adjusted to match with the GMR sensor, which helped reduce the background level of the Wheatstone bridge and increase the sensitivity of the measurement. The differential voltage of the Wheatstone bridge was fed into the lock-in and modulated with its internal reference signal. The processed analog output of the lock-in was transferred to a NI data acquisition box. A LabView computer program was used to collect the digital signal from the NI USB box.
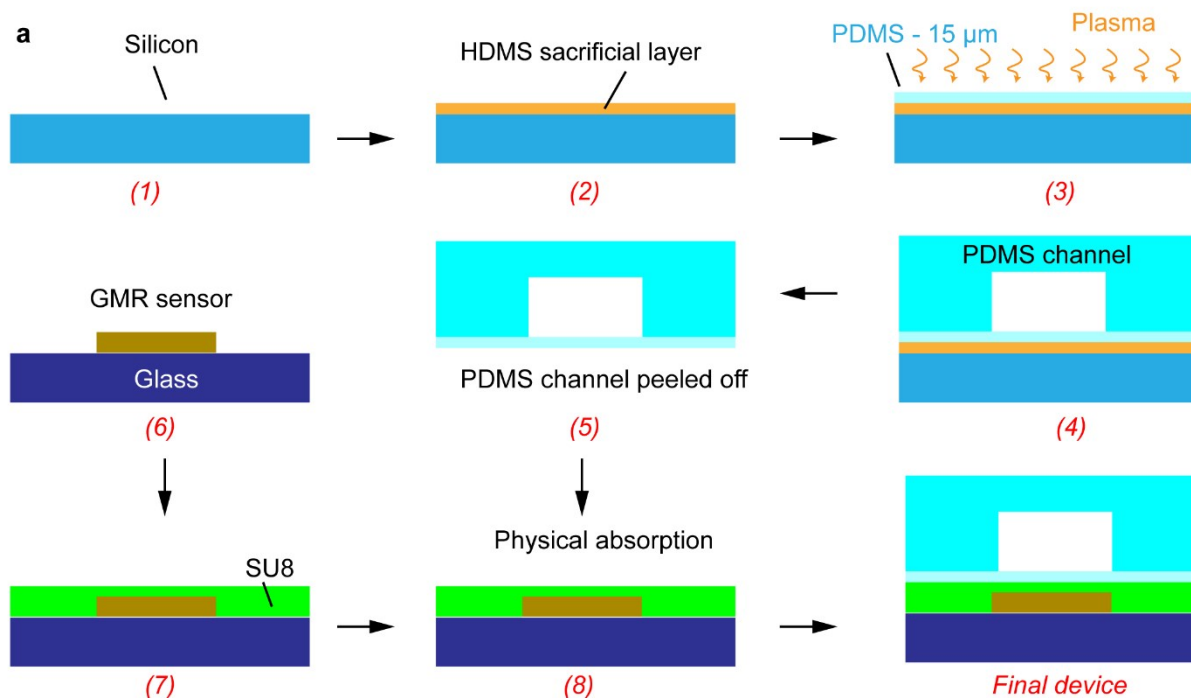
Figure S4 | Fabrication of a magnetofluidic decoder. The device was fabricated by assembling PDMS-based fluidic channel with a GMR sensor chip. For repeated use of the sensor chip, we used physical adsorption of a PDMS membrane between the PDMS fluidic channel and the sensor chip. The 15 μm membrane was fabricated by spin coating PDMS pre-polymers on a silicon substrate which was coated with a thin layer of HDMS as a sacrificial layer. Then the enclosed channel was fabricated by bonding the PMDS channel with the PDMS membrane. A 4μm SU-8 layer was deposited on the surface of the sensor to protect the sensor from shunting. After that, the whole channel was physically attached to the chip. The sensor was designed as a sensor stripe or a meander shape consisting of multiple stripes. The width and length of each GMR sensor stripe was 20 μm and 500 μm, respectively. The spacing between two sensor stripes was 20μm. The dimension of the channel for particle delivery is 500 μm x 500 μm x 500 μm.

Supplementary Section 4: DNA sequences for viruses used for biochemical assays

Virus	Capture DNA	Target DNA	Probe DNA
EV	5'-/5AmMC12/ATA CTG TTC TCC-3'	5'-GGA GTA AAT GTT GGA GAA CAG TAT -3'	5'-AAC ATT TAC TCC -C12- 3' - /36-TAMSp/-3'
HIV	5'-/5AmMC12/GTC ATG TTA TTC -3'	5'-AGA AGA TAT TTG GAA TAA CAT GAC-3'	5'-CAA ATA TCT TCT -C12- 3' - /36-TAMSp/- 3'
HCV	5'-/5AmMC12/CGT GTA AGT GAC -3'	5'-GGC GTT GAC GGG GTC ACT TAC ACG -3'	5'-CCC GTC AAC GCC -C12- 3' - /36-TAMSp/3'
HPV	5'-/5AmMC12/AAT GCT AGT GCT -3'	5'-ATT TGC TGC ATA AGC ACT AGC ATT -3'	5'-TAT GCA GCA AAT -C12- 3' - /36-TAMSp/-3'
HBV	5'-/5AmMC12/ATC ATC CAT ATA -3'	5'-TTG GCT TTC AGT TAT ATG GAT GAT -3'	5'-ACT GAA AGC CAA -C12- 3' - /36-TAMSp/-3'

Table S2 DNA sequences for viruses used for biochemical assay

Supplementary Section 5: Chracterization of magnetic material

Table S3 EFH1 Specifications and Physical Properties

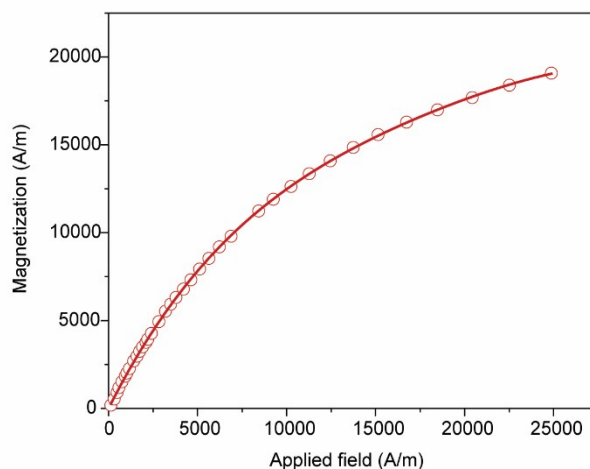| Appearance	Black-brown fluid
Carrier Liquid	Light Hydrocarbon
Saturation Magnetization (Ms)	44 mT
Viscosity @27°C	6 mPa·s
Density @25°C	$1.21\ 10^3$ kg/m^3
Pour Point	-94 °C
Flash Point	92 °C
Initial Magnetic Susceptibility	2.64

Figure S5 Magnetization vs applied magnetic field for EFH1 Ferrofluid. Magnetization data were determined using a vibrating sample magnetometer and were provided by Ferrotec, which was characterized by vibrating magnetometer[2].

References

1. Zhang, X., Huang, C. & Jin, X. Influence of K+ and Na+ ions on the degradation of wet-spun alginate fibers for tissue engineering. *J. Appl. Polym. Sci.* **134**, (2017).

2. Brandon A. Jackson;Lyon B. Kingb. Ferrofluid Interface Deformation and Spray Onset under Electric and Magnetic Stresses. *Am. Inst. Aeronaut. Astronaut.* https://pdfs.semanticscholar.org/37c0/cbc507ce4766